# Formation and Stability of Barium Aluminate and Cerate in $NO_x$ Storage-Reduction Catalysts

Maria Casapu[1], Jan-Dierk Grunwaldt[1,*], Marek Maciejewski[1], Meike Wittrock[2], Ulrich Göbel[2], Alfons Baiker[1,*]

[1]*Department of Chemistry and Applied Biosciences, Swiss Federal Institute of Technology, ETH Hönggerberg, CH-8093 Zürich, Switzerland*

[2]*Umicore AG & Co. KG, Rodenbacher Chaussee 4, D-63403 Hanau-Wolfgang, Germany*

* Corresponding authors.

*Email-addresses*: grunwaldt@chem.ethz.ch (J.-D. Grunwaldt), baiker@chem.ethz.ch (A. Baiker)

**Abstract**

The formation and stability of $BaAl_2O_4$ and $BaCeO_3$ in Pt-Ba/$Al_2O_3$ and Pt-Ba/$CeO_2$ based $NO_x$ storage-reduction (NSR) catalyst has been investigated using kinetic measurements, X-ray diffraction, thermal analysis and X-ray absorption spectroscopy. In as-prepared state, the Ba-component in the NSR catalysts was made up of amorphous BaO and $BaCO_3$. The formation of $BaAl_2O_4$ started above 850°C, whereas the formation of $BaCeO_3$ was already observed at 800°C and was faster than that of $BaAl_2O_4$. The stability of $BaAl_2O_4$ and $BaCeO_3$ in various liquid and gaseous atmospheres was different. $BaAl_2O_4$ was rapidly hydrated at room temperature in the presence of water and transformed to $Ba(NO_3)_2$ and γ-alumina in the presence of $HNO_3$, whereas $BaCeO_3$ was decomposed to much lower extent under these conditions. Interestingly, $BaCeO_3$ was transformed to $Ba(NO_3)_2$/$CeO_2$ in the presence of $NO_2$/$H_2O$ at 300 – 500 °C. Also the presence of $CO_2$ led to decomposition of barium cerate, which has important consequences for the catalyst ageing under $NO_x$-storage conditions and can be exploited for regeneration of thermally aged NSR-catalysts.

**Keywords:** $NO_x$ storage-reduction catalyst; Pt-Ba/$Al_2O_3$; Pt-Ba/$CeO_2$; barium aluminate; barium cerate; thermal stability; ageing; X-ray diffraction; thermal analysis; X-ray absorption spectroscopy; regeneration.

## 1. Introduction

The introduction of lean-burn engines with direct fuel injection is presently one of the most promising engine concepts to decrease fuel consumption [1-3]. The lean-burn engines, which operate at air-fuel ratios higher than 25:1, thus contribute to the conservation of fossil fuel reserves and thereby reduce the associated $CO_2$ emission. In Europe, the automotive industry is not only committed to reduce the average $CO_2$ emission level but also to clean up the exhaust gases at the same time. Following EU proposals further $CO_2$ emission reduction to 120 g/km shall be realized by 2012 [4]. However, neither the diesel exhaust catalyst nor the conventional three-way catalyst are able to reduce $NO_x$-emissions under lean conditions. Among the different strategies to reduce $NO_x$-emissions, the $NO_x$ storage-reduction (NSR) catalyst system is well-established because of its high lean $DeNO_x$ activity combined with a suitable durability and three-way catalyst activity [2, 5, 6].

NSR catalysts consist of precious metals (Pt, Rh) for the oxidation of NO to $NO_2$ (under lean fuel conditions) and reduction of $NO_x$ (under rich conditions), and of a storage component deposited on carrier oxides with a high surface area, such as $La_2O_3$-stabilized $\gamma$-$Al_2O_3$ or $CeO_2$ [5-10]. Typical $NO_x$ storage compounds are alkali metal oxides or alkaline-earth metal oxides like potassium oxide or barium oxide.

The $NO_x$ storage and reduction performance of such catalysts depends on various factors, including the dispersion of the noble metal and the Ba constituent as well as thermal stability, structural and textural properties. Deactivation of NSR catalysts is mainly caused by sulfur and thermal deterioration. Apart from the development of catalysts with higher tolerance of $SO_2$ or $SO_2$-derived species [11, 12], one of the major challenges is therefore the improvement of the thermal stability of NSR catalysts under

operating conditions. Thermal deterioration occurs both due to the particle growth of the precious metals and due to the formation of mixed oxides such as aluminates, cerates, and zirconates by the reaction of $NO_x$ storage material with the support or compounds in the wash-coat [8, 13-16].

Considerable effort has been made to elucidate elementary steps of the reaction mechanisms of storage and regeneration and the deterioration of the catalytic activity in the presence of sulfur containing gasses. In contrast, relatively little attention has been given to studies on the reaction of the storage material with the support during ageing and the stability of the formed phases in the presence of $NO_x$, $CO_2$, and $H_2O$ containing gases. Generally, the formation of barium aluminates and barium cerates is believed to have a negative influence on the $NO_x$ storage catalysts activity [8, 13, 14, 16]. However, in some articles a good potential of $Pt/BaAl_2O_4$ for $NO_2$ trapping has been reported [17, 18].

Here, we report a study on the formation and stability of barium aluminate and barium cerate in $Pt\text{-}Ba/Al_2O_3$ and $Pt\text{-}Ba/CeO_2$, respectively. The stability of these mixed oxide phases when exposed to different exhaust gas components, including $H_2O$, $NO_2$ and $CO_2$, has been studied systematically.

## 2. Experimental part

### *2.1. Sample preparation*

The $Pt\text{-}Ba/\gamma\text{-}Al_2O_3$ and $Pt\text{-}Ba/CeO_2$ samples were prepared using the following procedure. First, γ-alumina and ceria supports (Umicore) were calcined at 700°C for 5h. The surface area after calcination was 190 $m^2/g$ for $\gamma\text{-}Al_2O_3$ and 95 $m^2/g$ for $CeO_2$. Then platinum and barium were added in several steps to the supports by incipient wetness impregnation with aqueous solutions of dinitrodiamine platinum (Strem Chemicals) and barium acetate (Fluka). After each step the powders were dried overnight at 80°C and

then calcined at 500°C for 5h. The loadings of the noble metal and Ba were 1 and 17 wt%, respectively

To investigate the formation of $BaAl_2O_4$ and $BaCeO_3$, Pt-Ba/γ-$Al_2O_3$ and Pt-Ba/$CeO_2$ were calcined in a furnace (Nabertherm) in air at 800, 850, 900, 950 and 1000°C for different time periods between 2 to 10 h. The furnace was heated up in advance to the required temperature.

Additionally, another sample was prepared containing Pt supported on bulk $BaAl_2O_4$. by coprecipitation [19]. The corresponding amount of $Al(NO_3)_3 \cdot 9H_2O$ (ABCR) was dissolved in distilled water and the pH of the solution was adjusted to pH=1 with diluted $HNO_3$. Finally, the resulting solution was added under vigorous stirring to a 60°C heated $(NH_4)_2CO_3$ (ACROS) solution in large excess. The slurry was then aged for about 3h at 60°C and filtered off. After drying overnight, the solid material was calcined in air at 1000°C for 2h to form the $BaAl_2O_4$. This support was impregnated with a $H_2PtCl_6 \cdot 6H_2O$ (ABCR) solution, then dried and calcined in air at 500°C for 2h, the sample was denoted as "Pt/$BaAl_2O_4$".

*2.2. Reaction of $BaAl_2O_4$ and $BaCeO_3$ with $NO_2$, $H_2O$, and $CO_2$*

In order to test the reactivity of the formed mixed oxides towards $NO_2$ and $H_2O$, the samples with the highest content of barium aluminate and barium cerate (calcined for 10h at 1100°C and 1000°C, respectively) were exposed for different time periods to a flow of He saturated with water vapor (at room temperature) and 1 % $NO_2$ in synthetic air (1:1 mixture). The reaction temperature was varied between room temperature and 500°C.

The experiments were performed in a continuous-flow fixed-bed reactor. The reactor was filled with about 90 mg sample (pressed, ground and finally sieved). The sample was heated for 30 min to the selected temperature in a continuous flow of He. During reaction

the carrier gas (He) was first saturated with water at room temperature (~ 3 % $H_2O$) and then mixed with 1 % $NO_2$ in synthetic air. To avoid water condensation all pipes were heated. The flow rate was controlled by mass flow controllers (Brooks). The total flow was 50 ml/min: 25 ml/min water saturated He and 25 ml/min 1 % $NO_2$ in synthetic air. After a certain reaction time the sample was cooled to room temperature in He and analyzed.

The decomposition of $BaAl_2O_4$ and $BaCeO_3$ in $CO_2$ was studied by thermal analysis. The samples (ca. 70 mg) were heated with a rate of 10 K/min to 1300°C and cooled down with a rate of 5 K/min in 20, 15, 12.5 and 10 % $CO_2$ in He.

*2.3. Characterization techniques*

X-ray diffraction measurements were carried out on a Siemens D5000 powder X-ray diffractometer using the Cu $K_\alpha$ radiation in the step scanning mode between $2\Theta$ = 15 and 65°, with a step size of 0.01° and 2 s per step. For the quantification of the amount of barium aluminate and cerate in the samples the integral intensities (peak areas) of the reflections at $2\Theta$ = 28.3° ($BaAl_2O_4$) and $2\Theta$ = 40.9 and 41.1° ($BaCeO_3$) were compared with intensities of the reference samples containing only pure phases. The intensities were standardized by comparison with the inert standard i.e. the intensity of Cu (111) reflection at $2\Theta$ = 43.17°.

Thermal Analysis (TA, PulseTA [20]) experiments were performed on a Netzsch STA 409 thermoanalyser equipped with a pulse device enabling injection of a certain amount of one or two pure gases or gaseous mixtures into the carrier gas stream flowing through the system. The flow rate was controlled by mass flow controllers (Brooks model 5850E based on a thermal mass flow sensing technique). The thermoanalyser was

connected by a heated (ca. 200°C) stainless steel capillary to a Balzers quadrupole mass spectrometer QMG 420.

The BET surface area and pore size distribution were determined by $N_2$ adsorption-desorption using a Micromeritics ASAP 2010 instrument. Before measurement the samples were degassed in vacuum at 150° C.

EXAFS experiments were performed at the beamline X1 at HASYLAB in Hamburg, Germany. The storage ring typically operates at 4.45 GeV with a ring current between 80 and 120 mA. A Si(311) double-crystal was used as monochromator. The higher harmonics were removed by detuning of the crystals to 70% of the maximum intensity. EXAFS data were collected in the transmission mode at room temperature. Spectra were taken around the Ba K-edge (37.441 keV), using a $BaSO_4$ pellet as reference for energy calibration. For data evaluation the WINXAS 3.1 software was used [21]. Fourier transformation of the EXAFS data was applied on the $k^3$-weighted $\chi(k)$ data.

## 3. Results

### *3.1. $BaAl_2O_4$ and $BaCeO_3$ formation*

In the Ba-Al-O system, several Ba-Al oxides like $BaO{\cdot}Al_2O_3$ (barium mono-aluminate), $3BaO{\cdot}Al_2O_3$ (tri-barium mono-aluminate), $BaO{\cdot}6Al_2O_3$ (barium hexa-aluminate) as well as a number of nonstoichiometric aluminates were reported [22-24]. The formation of the phase is related either to the molar ratio between BaO and $Al_2O_3$ or to the preparation method and experimental conditions. In the Ba-Ce-O system, $BaCeO_3$ is reported to be the sole product formed by the reaction between BaO and $CeO_2$ [25]. In order to investigate the transformations during calcination both the Pt-$Ba/Al_2O_3$ and the Pt-$Ba/CeO_2$ samples were heated in the thermoanalyser with a rate of 10 K/min to 1300°C under an inert atmosphere (He).

In the Pt-Ba/$Al_2O_3$ model system, due to the excess of alumina, only $BaO{\cdot}Al_2O_3$ and $BaO{\cdot}6Al_2O_3$ can be formed. Fig. 1a depicts the X-ray diffraction patterns of the Pt-Ba/γ-$Al_2O_3$ sample in as-prepared state (pattern 1) and after calcination in the thermoanalyser up to 1200°C (just before the exothermic event on DSC curve in Fig. 2) and up to 1315°C. Note that in the as-prepared sample the BaO component exists as amorphous BaO and $BaCO_3$ [26, 27]. In the sample calcined up to 1200°C the characteristic reflections for $BaAl_2O_4$ appear while the $BaCO_3$ patterns disappear (Fig. 1a). The TG curve and the mass spectrometric signals recorded for $CO_2$ (*m/z* = 44) indicate that supported $BaCO_3$ starts to decompose at about 300°C. The maximum of $CO_2$ evolution is centered at about 637°C and the decomposition is finished at ca. 850°C. The amount of the $CO_2$ evolved was determined using pulse thermal analysis [20] by comparing the integral intensity of the $CO_2$ signal evolved during decomposition with the intensity of an injected pulse of 1 ml $CO_2$. Evolution of water from the support was only observed at low temperatures (< 200°C) and no thermal effect due to formation of $BaAl_2O_4$ was observed. Above 1220°C, $BaO{\cdot}6Al_2O_3$ was formed by a solid state reaction of $BaAl_2O_4$ and $Al_2O_3$. The characteristic reflections of $BaO{\cdot}6Al_2O_3$ are discernible in the XRD pattern of the sample heated to 1315°C (Fig. 1a). The formation of $BaO{\cdot}6Al_2O_3$ is also clearly visible on the DSC curve (Fig. 2a): the exothermic peak, centered at 1260°C, indicates the reaction between $Al_2O_3$ and $BaAl_2O_4$.

X-ray diffraction patterns taken after calcination of the Pt-Ba/$CeO_2$ sample in He at 1300°C, revealed the presence of $BaCeO_3$ as the only Ba-Ce mixed oxide (pattern 3 in Fig. 1b). The observed thermal effects during the process (Fig. 2b, DSC curve) uncovered a different course of the decomposition of $BaCO_3$ on the $CeO_2$ support compared to that on γ-$Al_2O_3$. $BaCO_3$ supported on cerium oxide seems to be more stable. There are two

maxima of $CO_2$ evolution (Fig. 2b), the first one at around 870°C and the second one centered at 1100°C. Also the DSC curve shows two distinct endothermic peaks due to $BaCO_3$ decomposition. Two small additional endothermic events with maxima at 810° and 976°C are due to the polymorphic transformation of not fully decomposed $BaCO_3$ at these temperatures. $BaCO_3$ transforms from orthorhombic to hexagonal structure at 803°C and to a cubic phase (NaCl structure) at 976°C [28].

During purification of the exhaust gases the operating temperature is lower than 500°C. Higher temperatures are reached during sulfur removal [29, 30] or due to the exothermic oxidation of hydrocarbons, CO and $H_2$. Nevertheless, in none of these processes the temperature exceeds 1000°C and therefore only $BaAl_2O_4$ and $BaCeO_3$ can be formed.

To examine the progress of formation of these phases, Pt-Ba/$Al_2O_3$ and Pt-Ba/$CeO_2$ samples were calcined for different time periods at temperatures between 800°C to 1000°C. At lower temperature Ba-Al-oxides could not be identified, as confirmed in a preliminary investigation: the X-ray diffraction patterns recorded for a mixture of $BaCO_3$ - $\gamma$-$Al_2O_3$ (with a molar ratio of 1) after calcination for 20h at 700°C did not indicate the characteristic reflections of $BaAl_2O_4$. Only at higher temperatures (cf. Fig. 3a), $BaAl_2O_4$ was detected. Similar results, regarding barium mono-aluminate formation (Fig. 3a), were reported in the literature [13, 14].

Phase identification and quantitative analysis of barium aluminate and barium cerate formation were performed by XRD. Figures 3a and 3b depict the XRD patterns of both catalysts after calcination at different temperatures. Formation of $BaCeO_3$ was already observed after calcination at 800°C while $BaAl_2O_4$ reflections are not detectable after treatment at this temperature. The yield of the formation of $BaAl_2O_4$ and $BaCeO_3$ as a

function of temperature and calcination time is presented in Figs. 4a and 4b, respectively. Note the significant differences in the formation of the two mixed oxide phases. For the sample calcined at 850°C for 8h more than half of the $BaCeO_3$ was already formed, whereas only traces of $BaAl_2O_4$ could be observed under these conditions.

The XANES/EXAFS technique was used to study the local structure of the calcined samples. The spectra were taken around Ba K-edge (37.441 keV) in transmission mode. While there were no evident changes in the XANES spectra of Pt/$BaAl_2O_4$-BaO/$Al_2O_3$ and Pt/$BaCeO_3$-BaO/$CeO_2$ samples, a clear variation in the extended X-ray absorption fine structure data was found during the formation of $BaAl_2O_4$ and $BaCeO_3$. The Fourier transformed EXAFS spectra reveal a more crystalline structure for $BaCeO_3$ in comparison with $BaAl_2O_4$ and also a faster rate of formation (Figs. 5a and 5b). The crystal structure of $BaAl_2O_4$ is known to be hexagonal [31, 32]. For $BaCeO_3$ Preda *et al.* [33] found the tetragonal structure at low temperature and cubic at high temperature, whereas Scherban *et al.* [34] reported that barium cerate undergoes two phase transitions from orthorhombic to tetragonal and tetragonal to cubic structures between 100°C and 1000°C. Using FEFF calculations (FEFF 6.0 code [35]) and its comparison to the experimental EXAFS data, it was found that the Pt-Ba/$CeO_2$ sample calcined above 1000°C contains $BaCeO_3$ with cubic crystal structure.

### *3.2. Behaviour of $BaAl_2O_4$ and $BaCeO_3$ in the presence of liquid $H_2O$ and diluted $HNO_3$*

In order to gain some information on the chemical stability of $BaAl_2O_4$ and $BaCeO_3$, reference samples were investigated during the treatment with $H_2O$ (l) and aqueous solution of $HNO_3$ (7.2 wt. %). These latter conditions are typical for impregnation, additionally their application can also helps in understanding the results presented in section 3.3. The reference barium cerate was obtained by calcination of the Pt-Ba/$CeO_2$

sample for 10h at 1000°C and the reference barium aluminate, due to its lower rate of formation, by calcination of the Pt-Ba/γ-$Al_2O_3$ sample at 1100°C. Their properties are depicted in Table 1. Although calcination for ten hours led to a significant decrease of the surface area of both samples, the Pt/$BaAl_2O_4$-BaO/γ-$Al_2O_3$ sample had still a high surface area (89 $m^2$/g) after calcination. This finding agrees well with observations that the presence of Ba inhibits the sintering and the phase transformation of γ-$Al_2O_3$ [36-41]. For Pt/$BaCeO_3$-BaO/$CeO_2$, the surface area decreased drastically to 3.7 $m^2$/g after calcination at 1000°C.

After the corresponding calcinations, the samples were treated with $H_2O$(l) or $HNO_3$ (7.2 wt. %) at room temperature and dried over night at 80°C. X-ray diffraction patterns recorded after treatment uncovered that barium aluminate and barium cerate were decomposed as a result of the reaction with $HNO_3$ (Fig. 6). The $BaAl_2O_4$ and $BaCeO_3$ reflections at 2Θ = 28.3° and 2Θ = 40.9 and 41.1°, respectively, decreased and typical reflections for $Ba(NO_3)_2$ and $BaCO_3$ were identified in the corresponding XRD patterns. While diluted nitric acid transformed barium aluminate in the aged catalyst completely to $Ba(NO_3)_2$ and γ-$Al_2O_3$ (Fig. 6a) a more concentrated solution of $HNO_3$ (or longer treatment) was required for $BaCeO_3$ to achieve the same effect (cf. Fig. 6b). A similar behavior during reaction with diluted $HNO_3$ was observed also for the bulk $BaAl_2O_4$ sample prepared by coprecipitation method.

The treatment of Pt/$BaAl_2O_4$-BaO/$Al_2O_3$ with pure water followed by drying at 80°C resulted in a total disappearance of XRD reflections of $BaAl_2O_4$ (Fig. 6a-2) while for Pt/$BaCeO_3$-BaO/$CeO_2$ no major changes (Fig. 6b-2) could be detected by XRD. Also the Pt/$BaAl_2O_4$ sample reacted with water. The X-ray pattern typical for $BaAl_2O_4$ diminished after impregnation with water and drying at 80°C over night (not shown). Carlson *et al.*

[42] reported that $BaAl_2O_4$ can be hydrolyzed by water. Furthermore, variousstructurally defined hydrates ($xBaO{\cdot}yAl_2O_3{\cdot}zH_2O$) were hydrothermally prepared [42-47].

In the present study, the samples after treatment with water were X-ray amorphous and therefore no characteristic XRD pattern for the hydrates (only carbonate) could be identified. However, TA-MS measurements showed the evolution of water in well-resolved steps indicating the formation of the hydrates after treatment of $Pt/BaAl_2O_4$ and $Pt/BaAl_2O_4$-$BaO/Al_2O_3$ with water. The mass loss amounted to 18.5% for $Pt/BaAl_2O_4$ and 10.6% for $Pt/BaAl_2O_4$-$BaO/Al_2O_3$, respectively (see Fig. 7). This corresponds to a molar ratio between $BaAl_2O_4$ and $H_2O$ of about 0.3 (three $H_2O$ molecules) and 0.17 (six $H_2O$ molecules), respectively. After reaction with water two endothermic events were observed between 50°C to 450°C during calcination of $Pt/BaAl_2O_4$ samples and for $Pt/BaAl_2O_4$-$BaO/Al_2O_3$ samples between 50°C and 290°C (Figs. 7a and 7b). According to the report by Budnikov *et al.* [48] we assign these peaks to the dehydration of $BaO{\cdot}Al_2O_3{\cdot}7H_2O$ or $BaO{\cdot}Al_2O_3{\cdot}6H_2O$ to $BaO{\cdot}Al_2O_3{\cdot}H_2O$ (up to 140°C) and to dehydration of $BaO{\cdot}Al_2O_3{\cdot}H_2O$, which occurs at higher temperatures. The mass spectrometric signal of m/z= 18 in Fig. 7 shows that the evolution of water is complete at about 850°C. At 829°C an exothermic signal on the DSC curve is observed. The XRD patterns of the $Pt/BaAl_2O_4$ hydrated sample which was heated to 690°C (before the exothermic peak) revealed the presence of only small traces of $BaAl_2O_4$ while in the sample heated to 890°C the corresponding characteristic XRD reflections were very sharp (not shown). This observation agrees well with suggestions of Ahmed et al. and Budnikov et al. [43, 48] that the dehydration of the monohydrate in which water has been ascribed “zeolitic properties”, does not lead to the formation of the crystal structure of anhydrous barium aluminate below 750°C. The crystallization of the poorly crystalline

barium aluminate after evolution of this residual water occurred between ca. 750 – 850 °C, indicated by an exothermic peak in the DSC curve (Fig. 7a). No difference could be observed in the XRD patterns of $Pt/BaAl_2O_4$ hydrate calcined up to 1200°C in comparison with the XRD of the sample after the crystallization event (at 890°C).

The DSC curve recorded during $Pt/BaAl_2O_4$-$BaO/Al_2O_4$ hydrate calcination under inert atmosphere (He) did not show the exothermic peak above 800°C (see Fig. 7b). Also the X-ray diffraction patterns of the sample calcined up to 800°C did not contain any reflection indicating $BaAl_2O_4$. For a sample calcined up to 910°C characteristic XRD patterns of $BaAl_2O_4$ could be identified.

*3.3. $BaAl_2O_4$ and $BaCeO_3$ reaction with $H_2O$ and $NO_2$ in gas phase*

Next, the stability of $BaAl_2O_4$ and $BaCeO_3$ was investigated in the presence of $NO_2$ and water (gas phase) at elevated temperature in a continuous-flow fixed-bed reactor using a 1:1 mixture of 1%$NO_2$/synthetic air and ~3%$H_2O$/He. A temperature of 300°C was chosen as starting point since it lies in the temperature range where the NSR catalysts reach their maximal performance and thus reasonable $NO_x$ conversion and stability against sintering can be expected [49-52]. After defined time intervals the reaction progress was investigated by XRD; the results are depicted in Fig. 8. Additionally, the samples were characterized by temperature-programmed decomposition experiments in an inert atmosphere (He). The typical mass changes (TG curve) and the intensities of the mass spectrometric signals of $CO_2$ and NO ($O_2$ has also been recorded, not shown) during decomposition of the $Pt/BaCeO_3$-$BaO/CeO_2$ sample after reaction with $NO_2$ and $H_2O$ at 300°C for 7h are depicted in Fig. 9. The amount of NO, $CO_2$ and $O_2$ evolved was determined by pulse thermal analysis. For this purpose 1 ml pulses of NO, $CO_2$ and $O_2$ were injected after the decomposition of $BaCO_3$ and $Ba(NO_3)_2$. Their intensity was

compared to the corresponding integral intensity during decomposition in order to calculate the amount of the barium carbonate and nitrate. This allowed determining the progress of the reaction between $BaAl_2O_4$ or $BaCeO_3$ and $NO_2$ in the water saturated atmosphere.

The fraction of barium present in form of $BaCO_3$ in $Pt/BaAl_2O_4$-$BaO/Al_2O_3$ and $Pt/BaCeO_3$-$BaO/CeO_2$ before reaction with $NO_2$ and $H_2O$ was calculated from the amount of evolved $CO_2$ during temperature-programmed decomposition. Assuming that Ba in the sample is only present as $BaCO_3$ and mixed oxides this allows determining the $BaAl_2O_4$ and $BaCeO_3$ amount present in the samples before the reaction with $H_2O$ and $NO_2$. Comparing this amount with that in the sample after reaction including the amount of Ba in the form of $Ba(NO_3)_2$ after reaction, the progress of the reaction between $BaAl_2O_4$ or $BaCeO_3$ and $NO_2$ in water saturated atmosphere at 300°C could be calculated as a function of time as shown in Fig. 10.

$BaCeO_3$, which was formed more easily than $BaAl_2O_4$, decomposed in $NO_2/H_2O$ atmosphere around 300°C. After reaction with $NO_2$ in $H_2O$ saturated atmosphere for ca. 7 h at 300°C all $BaCeO_3$ was converted to $Ba(NO_3)_2$. Fig. 8b depicts the XRD patterns for $Pt/BaCeO_3$-$BaO/CeO_2$ sample before and after a certain reaction time at 300°C. The characteristic reflections of $BaCeO_3$ disappeared rather fast; after 1 h reaction time only a small amount of crystalline $BaCeO_3$ remained. The progress of $BaCeO_3$ decomposition calculated from XRD for different conditions and temperatures is shown in Fig. 10b. TA-MS investigations gave similar results. For comparison, a result obtained by TG-MS for the reaction at 300°C is shown in Fig. 10b (dotted line) as well. The reaction of $BaCeO_3$ with water saturated He (~3% $H_2O$/He) in the absence of $NO_2$ was slower than in the presence of $NO_2$. However, after 5h the barium cerate was also significantly decomposed.

Obviously, the $Ba(NO_3)_2$ formed in presence of $NO_2$ shifted the reaction equilibrium between $BaCeO_3$ and $H_2O$ towards the products thus enhancing the reaction progress.

In a next step, we extended our study regarding the stability of barium cerate to higher temperature. The XRD results shown in Fig. 10b indicate that at 400°C the reaction is faster than at 300°C while at 500°C the conversion of $BaCeO_3$ decreases. This is supported by corresponding TA-MS results. One explanation is that at higher temperature $Ba(NO_3)_2$ is unstable and therefore it cannot be formed. Its decomposition starts under non-isothermal conditions at about 400°C according to Fig. 9. Thus the progress of reaction between $BaCeO_3$ and $H_2O$ at 500°C is less affected by the presence of $NO_2$.

The instability of $BaAl_2O_4$ in the presence of water found at room temperature was not observed at higher temperature. After 8h reaction with $H_2O$ and $NO_2$ at 300°C, the characteristic XRD patterns for $Ba(NO_3)$ appeared but there was no change in the intensity of the reflections due to $BaAl_2O_4$. These observations were also verified by TA-MS experiments. $Ba(NO_3)_2$ formed by reaction between $NO_2$ and BaO or $BaCO_3$ that remained in the sample after calcination due to incomplete transformation to $BaAl_2O_4$ (Fig. 8a). At 400°C also no $BaAl_2O_4$ reaction was found and in this case no $Ba(NO_3)$ was present, since it is not stable at this temperature (Fig. 8a).

Based on these observations and the fact that at room temperature $BaAl_2O_4$ was completely decomposed by liquid water and diluted $HNO_3$, additional experiments were carried out in the range of 30 – 100 °C. In fact, it was observed that the XRD reflections of $BaAl_2O_4$ disappeared during treatment with water saturated He at such low temperatures. The study of the $BaAl_2O_4$ decomposition at 100°C, 50°C and 30°C uncovered that $BaAl_2O_4$ reacted particularly at low temperature in a gaseous 1:1 mixture

of 3% $H_2O$/He and 1% $NO_2$/synthetic air. Fig. 8a depicts the X-ray diffraction patterns for as-prepared sample and after 4h reaction at 30°C. The results of corresponding TA-MS experiments are summarized in Fig. 10a. The reaction progress calculated from the TG-MS measurements revealed the slowing down of the reaction with increasing temperature.

Finally, we observed that storing the Pt/$BaAl_2O_4$-BaO/γ-$Al_2O_3$ sample in air for a longer time period led to a decrease of X-ray reflections of $BaAl_2O_4$, whereas the $BaCO_3$ reflections increased in intensity (not shown). This observation is in accordance with the results previously described and indicates the slow hydration of $BaAl_2O_4$ at room temperature by water from the ambient atmosphere.

*3.4. Reaction of $BaAl_2O_4$ and $BaCeO_3$ with $CO_2$*

Due to the fact that the exhaust gases contain a significant amount of $CO_2$ and since it was reported that pure $BaCeO_3$ can be decomposed in the presence of $CO_2$ [53, 54] we studied the behavior of Pt/$BaAl_2O_4$-BaO/γ-$Al_2O_3$ and Pt/$BaCeO_3$-BaO/$CeO_2$ samples during heating to 1300°C and cooling in $CO_2$/He atmosphere. The TG curves recorded during experiments are presented in Fig. 11. $BaAl_2O_4$ did not react with $CO_2$. The mass loss during heating in 20%$CO_2$/He is due to evolution of water and $BaCO_3$ decomposition. No mass uptake occurred during cooling down, the apparent mass change between 100°- 1200°C resulted from the buoyancy effect.

Pt/$BaCeO_3$-BaO/$CeO_2$ in $CO_2$ atmosphere behaved differently. In 20 vol% $CO_2$/He the sample mass increased distinctly between ca. 400°C and 980°C indicating decomposition of $BaCeO_3$ and reaction of formed BaO with $CO_2$. Above 980°C, $BaCeO_3$ was formed again by the reaction of $BaCO_3$ with $CeO_2$ with a mass loss due to $CO_2$ evolution. During cooling (Fig. 11b) $BaCeO_3$ decomposed again. The XRD patterns

recorded for Pt/$BaCeO_3$-BaO/$CeO_2$ after heating to 950°C in 20 %$CO_2$/He revealed the formation of $BaCO_3$ and $CeO_2$ by decomposition of $BaCeO_3$ (not shown). At lower $CO_2$ concentration the reaction between $BaCeO_3$ and $CO_2$ occurred to lesser extent and was shifted to higher temperature while the reaction of formed $BaCO_3$ with $CeO_2$ was shifted to lower temperature. Therefore the temperature range of the $BaCeO_3$ reaction with $CO_2$ became narrower under dynamic reaction conditions at lower $CO_2$ concentration (Fig. 11b).

## 4. Discussion

The systematic study brought new insight into the formation and decomposition of undesired barium aluminate and barium cerate in NSR catalysts. The stability of these mixed oxides is affected by the presence of carbon dioxide, $NO_x$ and water. Both barium aluminate and barium cerate form during reaction of the $NO_x$ storage material (BaO / $BaCO_3$) and the support ($\gamma$-$Al_2O_3$ or $CeO_2$) at elevated temperature. The results show that the formation of barium cerate occurs much faster and at lower temperature (800°C) compared to barium aluminate (> 850°C). However, barium cerate is less stable and decomposes in the presence of carbon dioxide, $NO_x$ and water at 300 – 500 °C. Proper knowledge of these interdependencies is a necessary prerequisite for understanding and controlling the processes during operation and for regeneration of NSR catalysts.

With respect to the formation of barium aluminate in Pt-Ba/$\gamma$-$Al_2O_3$ the results correspond well to previous studies on the reaction of BaO and $\gamma$-$Al_2O_3$ that was reported to occur above 800°C when barium ($Ba^{2+}$) and oxygen ions ($O^{2-}$) can migrate into the alumina [55]. $BaCO_3$ in the as-prepared Pt-Ba/$\gamma$-$Al_2O_3$ starts to decompose at about 300°C, i.e. at much lower temperature than bulk $BaCO_3$ (decomposition starts above 800°C) and it is completely decomposed at ca. 850°C. A similar behaviour was found for

$BaCO_3$ deposited on other supports [26]. Hence, the $BaCO_3$ present in the as-prepared catalyst is already decomposed, when $BaAl_2O_4$ formation starts. Since the Pt-Ba/γ-$Al_2O_3$ sample used in our study contained excess of $Al_2O_3$ at higher temperature (> 1260°C) the formation of another Ba-Al-oxide with a BaO:$Al_2O_3$ composition of 1:6 was observed.

In Pt-Ba/$CeO_2$, the decomposition of $BaCO_3$ occurs in two steps and is superimposed by two polymorphic transformations of barium carbonate at 809 °C and at 976°C. In comparison to Pt-Ba/γ-$Al_2O_3$ the decomposition of $BaCO_3$ supported on ceria proceeds at higher temperature, probably due to the lower dispersion of the barium containing species on the support. Moreover, the formation of $BaCeO_3$ occurs simultaneously with $BaCO_3$ decomposition and is much faster than that of $BaAl_2O_4$ (Fig. 3). $BaAl_2O_4$ was mainly formed after the complete decomposition of $BaCO_3$. The EXAFS data confirm the faster rate of $BaCeO_3$ formation compared to that of $BaAl_2O_4$, and also the higher crystallinity of Ba-compounds on ceria than on alumina.

Our studies also indicate that the formation and stability of barium aluminate and barium cerate is affected by the presence of carbon dioxide, $NO_x$ and water. Calcination experiments alone are not sufficient to understand the formation of the undesired mixed oxides. Only a few studies exist that report the behaviour of bulk $BaCeO_3$ in the presence of water [54] and $CO_2$ [53], respectively. While in vehicle exhaust gases $CO_2$, $H_2O$, $NO_x$, CO, $SO_x$, and unburned hydrocarbons are present, we restricted our studies here to model gas compositions containing $NO_2$, $H_2O$ and $CO_2$. In the presence of nitric acid and $H_2O$ (l), $BaAl_2O_4$ as bulk material or supported on $Al_2O_3$ exhibited a higher reactivity towards nitric acid or pure water than $BaCeO_3$. $BaAl_2O_4$ was formed more easily and the emerging phases decomposed more rapidly when finely dispersed on $Al_2O_3$, probably due to the higher surface area of Pt/$BaAl_2O_4$-BaO/γ-$Al_2O_3$ compared to Pt/$BaAl_2O_4$. In both

cases the residual water was liberated up to 800°C and after removal of all water from the hydrated sample conversion back to $BaAl_2O_4$ occurred. In the presence of $HNO_3$ the hydrates were further converted to $Ba(NO_3)_2$ and $Al_2O_3$.

While $BaCeO_3$ is hardly hydrated at room temperature and shows an increased stability towards $HNO_3$ exposure (Fig. 6b), $BaCeO_3$ reacts easier in the presence of gaseous $H_2O$ and $NO_2$ or carbon dioxide at elevated temperatures. $BaAl_2O_4$ does not react with $H_2O$ in presence or absence of $NO_2$ in the temperature interval 300 – 500 °C (Figs. 9a and 9b). The reaction between $BaCeO_3$ and $H_2O$ is accelerated in presence of $NO_2$ probably through $Ba(NO_3)_2$ formation and reaches a maximum rate at 400°C (Fig. 10b). Above 450 °C $Ba(NO_3)_2$ is decomposed. Therefore the reaction equilibrium is not influenced anymore by the presence of $NO_2$. $BaAl_2O_4$ in the aged Pt-Ba/$Al_2O_3$ material can be also decomposed in a $H_2O/NO_2$ atmosphere but, in contrast to Pt/$BaCeO_3$ only at low temperatures. Below 100°C barium aluminate is hydrated easily resulting in the formation of barium aluminate hydrates. These compounds, being intermediate phases, react further with $NO_2$ yielding $Ba(NO_3)_2$ and γ-$Al_2O_3$ as final products. $CO_2$ was further found to react with $BaCeO_3$ in the aged Pt-Ba/$CeO_2$ sample but not with $BaAl_2O_4$ in aged Pt-Ba/γ-$Al_2O_3$. The temperature range for the reaction between $BaCeO_3$ and $CO_2$ becomes narrower at lower $CO_2$ concentrations.

These studies show that the $CO_2$ or water/$NO_2$ will strongly influence the presence of undesired $BaCeO_3$ in NSR catalysts. Note that the studies reported here were performed under static conditions. Similar studies under dynamic conditions will be required as well to gain a complete understanding of the impact of the observed phenomena on catalyst lifetime and regeneration. Nevertheless, the present observations under static conditions are already technically useful. The treatment of thermally aged Pt-Ba/γ-$Al_2O_3$

and Pt-Ba/$CeO_2$ catalysts in water, $NO_2$ or $CO_2$ could be exploited to decompose the undesired mixed oxides $BaAl_2O_4$ and $BaCeO_3$. In case of Pt-Ba/$CeO_2$ reaction with $NO_x$, $H_2O$ or $CO_2$ at 300 – 500 °C could be used, whereas in the Pt-Ba/γ-$Al_2O_3$ system lower temperatures would be beneficial for reactivation of thermally aged NSR catalysts. In fact, recent studies have shown a significant reactivation effect when a thermally aged barium cerium oxide system was exposed to the lean fuel conditions for a longer time [56].

## 5. Conclusions

The present systematic investigation provided new insight into the formation and decomposition of barium aluminate and barium cerate, processes which can greatly affect the $NO_x$ storage-regeneration activity. Simple heat impact, as mimicked by calcinations at higher temperature led to the formation of the undesired binary metal oxides. The formation and decomposition of these mixed oxides is strongly affected by the presence of water, $CO_2$ and $NO_2$. An important finding is the high instability of $BaCeO_3$ in the presence of $NO_2$/$H_2O$ or carbon dioxide at 300 – 500 °C. This may also explain the high stability of the $CeO_2$ support during $NO_x$-storage/reduction against the formation of a binary oxides. A potential technical application emerging from our studies is that the instability of the undesired mixed oxides when exposed to exhaust gas components may be utilized for regeneration of thermally aged catalysts. Studies towards this aim are presently pursued in our laboratories.

## 6. Acknowledgements

M.C. gratefully acknowledges financial support by Umicore Co&KG, also for the beamtime allocations at HASYLAB (DESY, Hamburg). We thank the beamline staff at beamline X1 as well as Stefan Hannemann and Matteo Caravati (ETH Zürich) for the support during our EXAFS measurements.

**References:**


[1] R. M. Heck and R. J. Farrauto, *Catalytic Air Polution Control*, R. van Nostrand, New York, **1995**.
[2] K.-H. Glück, U. Göbel, H. Hahn, J. Höhne, R. Krebs, T. Kreuzer and E. Pott, MTZ 61 (2000) 6.
[3] R. Krebs, L. Spiegel and B. Stiebels, in *8. Aachener Kolloquium Fahrzeug- und Motorentechnik*, Aachen, **1999**.
[4] *Auto-Jahresbericht des VDA*, **2004**.
[5] N. Takahashi, H. Shinjoh, T. Iijima, T. Suzuki, K. Yamazaki, K. Yokota, H. Suzuki, N. Miyoshi, S. Matsumoto, T. Tanizawa, T. Tanaka, S. Tateishi and K. Kasahara, Catal. Today 27 (1996) 63.
[6] W. Bögner, M. Krämer, B. Krutzsch, S. Pischinger, D. Voigtländer, G. Wenninger, F. Wirbeleit, M. S. Brogan, R.J. Brisley and D.E. Webster Appl. Catal. B 7 (1995) 153.
[7] N. Miyoshi, T. Tanizawa, K. Kasahara and S. Tateishi, SAE Tech. Paper 950809 (1995), *European Patent Application EP 0 669 157 A1*, **1995**.
[8] S. Matsumoto, CATTECH 4 (2000) 102.
[9] E. Fridell, H. Persson, B. Westerberg, L. Olsson and M. Skoglundh, Catal. Lett. 66 (2000) 71.
[10] S. Salasc, M. Skoglundh and E. Fridell, Appl. Catal. B 36 (2002) 145.
[11] P. Engstrom, A. Amberntsson, M. Skoglundh, E. Fridell and G. Smedler, Appl. Catal. B 22 (1999) L241.
[12] K. Wilson, C. Hardacre,C. J. Baddeley, J. Ludecke, D. P. Woodruff and R. M. Lambert, Surf. Sci. 372 (1997) 279.
[13] N. Fekete, R. Kemmler, D. Voigtländer, B. Krutzsch, E. Zimmer, G. Wenniger, W. Strehlau, J. A. A. v. d. Tillaart, J. Leyrer, E. S. Lox and W. Müller, SAE Tech. Paper 970746 (1997).
[14] B.-H. Jang, T.-H. Yeon, H.-S. Han, Y.-K. Park and J.-E. Yie, Catal. Lett. 77 (2001) 21.
[15] S. Elbouazzaoui, X. Courtois, P. Marecot and D. Duprez, Topics Catal. 30-31 (2004) 493.
[16] U. Göbel, J. Höhne, E. Lox, W. Müller, A. Okumura and L. Ruwisch, SAE Tech. Paper 99011285 (2000).
[17] S. Hodjati, P. Bernhardt, C. Petit, V. Pitchon and A. Kiennemann, Appl. Catal. B 19 (1998) 221.
[18] S. Hodjati, P. Bernhardt, C. Petit, V. Pitchon and A. Kiennemann, Appl. Catal. B 19 (1998) 209.
[19] G. Groppi, M. Bellotto, C. Cristiam, P. Forzatti and P. L. Villa, Appl. Catal. A 104 (1993) 101.
[20] M. Maciejewski, W. D. Emmerich and A. Baiker, J. Thermal Anal. Calorim. 56 (1999) 627.
[21] T. Ressler, J. Synchr. Rad. 5 (1998) 118.
[22] L. Perier-Camby and G. Thomas, Solid State Ionics 63-65 (1993) 128.
[23] L. Perier-Camby and G. Thomas, Solid State Ionics 93 (1997) 315.
[24] G. Groppi, C. Cristiam and P. Forzatti, J. Mat. Sci. 29 (1994) 3441.
[25] J. P. Guha and D. Kolar, J. Mat. Sci. 6 (1971) 1174.

[26] M. Piacentini, M. Maciejewski, T. Bürgi and A. Baiker, Topics Catal. 30/31 (2004) 71.
[27] M. Piacentini, M. Maciejewski and A. Baiker, Applied Catal. B 59 (2005) 187.
[28] J. J. Lander, J. Chem. Phys. 17 (1949) 892.
[29] S. I. Matsumoto, Y. Ikeda, H. Suzuki, M. Ogai and N. Miyoshi, Appl. Catal. B 25 (2000) 115.
[30] S. Poulston and R. R. Rajaram, Catal. Today 81 (2003) 603.
[31] R. Hoppe and B. Schepers, Naturw. 47 (1960) 376.
[32] W. Hoerkner and H. Mueller-Buschbaum, Z. Anorg. Allg. Chem. 451 (1979) 40.
[33] M. Preda and R. Dinescu, Rev. Roum Chim. 21 (1976) 1023.
[34] T. Scherban, R. Villeneuve, L. Abello and G. Lucazeau, Solid State Comm. 84 (1992) 341.
[35] M. Newville, B. Ravel, D. Haskel, J. J. Rehr, E. A. Stern and Y. Yacoby, Physica B: Condensed Matter 208-209 (1995) 154.
[36] P. Burtin, J. P. Brunelle, M. Pijolat and M. Soustelle, Appl. Catal. 34 (1987) 225.
[37] P. Burtin, J. P. Brunelle, M. Pijolat and M. Soustelle, Appl. Catal. 34 (1987) 239.
[38] J. S. Church, N. W. Cant and D. L. Trimm, Appl. Catal. A 107 (1994) 267.
[39] S. Rossignol and C. Kappenstein, Int. J. Inorg. Mat. 3 (2001) 51.
[40] H. K. Kang, S. S. S. M. M. Park, H. S. Lee and H. C. Park, Brit. Ceramic Trans. 99 (2000) 26.
[41] J. M. Schwaller, P. Wehrer, F. Garin and G. Maire, Ann.Chim. Fr. 14 (1989) 209.
[42] E. T. Carlson, T. J. Chaconas and L. S. Wells, J. Res. Nat. Bureau Stand. 45 (1950) 381.
[43] A. H. M. Ahmed and L. S. Dent Glasser, J. Appl. Chem. Biotechnol. 21 (1971) 107.
[44] A. H. M. Ahmed and L. S. Dent Glasser, J. Appl. Chem. Biotechnol. 21 (1971) 103.
[45] A. H. M. Ahmed, L. S. Dent Glasser and M. G. King, Acta Cryst. B29 (1973) 1166.
[46] M. C. Cruickshank, L. S. Dent Glasser and R. A. Howie, Acta Cryst. C41 (1985) 159.
[47] L. S. Dent Glasser and R. Giovanoli, Acta Cryst. B28 (1972) 519.
[48] P. P. Budnikov and V. G. Savelev, Silikaty 6 (1962) 329.
[49] H. Mahzoul, J. F. Brilhac and P. Gilot, Appl. Catal. B 20 (1999) 47.
[50] L. Lietti, P. Forzatti, I. Nova and E. Trocono, J. Catal. 204 (2001) 175.
[51] W. S. Epling, G. C. Campbell and J. E. Parks, Catal. Lett. 90 (2003) 45.
[52] E. Fridell, M. Skoglundh, B. Westerberg, S. Johansson and G. Smedler, J. Catal. 183 (1999) 196.
[53] M. J. Scholten, J. Schoonman, J. C. van Miltenburg and H. A. J. Oonk, Solid State Ionics 61 (1993) 83.
[54] C. W. Tanner and A. V. Virkar, J. Electrochem. Soc. 143 (1996) 1386.
[55] L. Perier-Camby, A. M. Vernay and G. Thomas, Mat. Sci. Forum 79-82 (1991) 671.
[56] M. Casapu, J.-D. Grunwaldt, M. Maciejewski, U. Göbel, T. Kreuzer, M. Wittrock, A. Baiker, in preparation.

Table 1. $Pt/BaAl_2O_4$-$BaO/\gamma$-$Al_2O_3$ and $Pt/BaCeO_3$-$BaO/CeO_2$ model systems

| **Model system** | **Precursor** | **BET surface area of the precursor ($m^2/g$)** | **Composition** | | **Calcination temperature (°C)** | **Calcination time (h)** | **BET surface area after calcination ($m^2/g$)** |
|---|---|---|---|---|---|---|---|
| | | | **Ba (%m/m)** | **Pt (%m/m)** | | | |
| **$Pt/BaAl_2O_4$-$BaO/\gamma$-$Al_2O_3$** | Pt-Ba/ $\gamma$-$Al_2O_3$ | 128 | 15.5 ± 0.2 | 0.735±0.008 | 1100 | 10 | 89 |
| **$Pt/BaCeO_3$-$BaO/CeO_2$** | Pt-Ba/ $CeO_2$ | 55 | 15.4 ± 0.2 | 0.746 ± 0.008 | 1000 | 10 | 3.7 |

**Figure Captions**

Fig. 1: a) Ba-Al-oxides formation evidenced by X-ray diffraction patterns of the Pt-Ba/γ-$Al_2O_3$ system: (1) as-prepared, (2) after heating to 1200°C and (3) 1315°C (∇: $BaCO_3$, •: γ-$Al_2O_3$, *: $BaAl_2O_4$ and ♦: $BaAl_{12}O_{19}$).

b) $BaCeO_3$ formation. XRD pattern of the Pt-Ba/$CeO_2$ system: (1) as-prepared (2) after calcination at 1000°C for 10h and (3) after heating with a rate of 10K/min to 1315°C (∇: $BaCO_3$, •: $CeO_2$, ♦: $BaCeO_3$, o: Platinum and □ Cu-reference).

Fig.2: Mass loss (TG), thermal effects (DSC) and intensity of mass spectrometric signals of $CO_2$ (m/z = 44) and $H_2O$ (m/z = 18) during calcination of (a) Pt-Ba/γ-$Al_2O_3$ and (b) Pt-Ba/$CeO_2$ in He (50 ml/min, rate of 10 K/min).

Fig. 3: $BaAl_2O_4$ and $BaCeO_3$ formation as a function of temperature illustrated by XRD of (a) as-prepared Pt-Ba/γ-$Al_2O_3$ (raw) and the samples calcined for 4h at 850°C, 950°C and 1000°C (∇: $BaCO_3$, •: γ-$Al_2O_3$, *: $BaAl_2O_4$, o: Platinum and □ Cu-reference), and (b) as-prepared Pt-Ba/$CeO_2$ (raw) and calcined for 4h at 800°C, 900°C and 950°C (∇: $BaCO_3$, •: $CeO_2$, ♦: $BaCeO_3$ and □ Cu-reference).

Fig. 4: $BaAl_2O_4$ and $BaCeO_3$ content in (a) Pt-Ba/γ-$Al_2O_3$ and (b) Pt-Ba/$CeO_2$ as a function of time and temperatures. The quantification was performed by XRD measurements (the used reflections are 2Θ = 28.3° for $BaAl_2O_4$ and 2Θ = 40.9 and 41.1° for $BaCeO_3$).

Fig. 5: Fourier transformed EXAFS spectra at the Ba K-edge of (top) Pt-Ba/γ-$Al_2O_3$ sample (raw material and after different calcinations temperatures) and (bottom) Pt-Ba/$CeO_2$ sample (raw material and after calcinations).

Fig. 6: Change of XRD patterns of (a) Pt/$BaAl_2O_4$-BaO/γ-$Al_2O_3$ (∇: $BaCO_3$, •: γ-$Al_2O_3$, *: $BaAl_2O_4$, ◊ $Ba(NO_3)_2$ and □ Cu-reference) and (b) Pt/$BaCeO_3$-BaO/$CeO_2$ (∇: $BaCO_3$, •: $CeO_2$, ♦: $BaCeO_3$, ◊ $Ba(NO_3)_2$ and □ Cu-reference) during treatment with different liquid solutions: (1) raw material, (2) after impregnation with $H_2O$ and drying over night at 80°C, (3) after reaction with $HNO_3$ solution (7.2 wt.%).

Fig. 7: Mass changes (TG), thermal effects (DSC) and intensity of mass spectrometric signals of $CO_2$ (m/z = 44) and $H_2O$ (m/z = 18) recorded during calcinations with a rate of 10 K/min of (a) hydrated Pt/$BaAl_2O_4$ and (b) hydrated Pt/$BaAl_2O_4$-BaO/$Al_2O_3$ in an inert atmosphere (He, 50 ml/min).

Fig. 8: a) XRD patterns of $Pt/BaAl_2O_4$-$BaO/\gamma$-$Al_2O_3$ sample before (1) and after reaction at 400°C (2), 300°C (3) and room temperature (4) for 4h with $NO_2$ in $H_2O$ saturated atmosphere (∇: $BaCO_3$, •: $\gamma$-$Al_2O_3$, *: $BaAl_2O_4$, ◊ $Ba(NO_3)_2$ and □ Cu-reference); b) XRD patterns for $Pt/BaCeO_3$-$BaO/CeO_2$ sample before and after reaction at 300°C with $NO_2$ in $H_2O$ saturated atmosphere (♦: $BaCeO_3$, ◊ $Ba(NO_3)_2$ and □ Cu-reference).

Fig. 9: Change of the mass (TG) and intensity of mass spectrometric signals of NO (m/z=30) and $CO_2$ (m/z=44) recorded during calcination of $Pt/BaCeO_3$-$BaO/CeO_2$ after reaction with $NO_2$ in $H_2O$ saturated atmosphere for 7h at 300°C (inert He atmosphere, heating rate 10 K/min).

Fig. 10: a) Progress of $BaAl_2O_4$ decomposition by reaction with $H_2O$ and $NO_2$ calculated from TA-MS measurements (■ 30°C; ▲ 50°C; ●100°C ○300°C);
b) Progress of $BaCeO_3$ decomposition by reaction with $H_2O$ in presence or absence of $NO_2$ calculated from XRD (—) and TA-MS (····) measurements (● $H_2O$ and $NO_2$ at 300°C (XRD);○ $H_2O$ and $NO_2$ at 300°C (TA-MS);▲$H_2O$ and $NO_2$ at 400°C (XRD); ■ $H_2O$ and $NO_2$ at 500°C (XRD);♦only $H_2O$ at 300°C (XRD)).

Fig. 11: a) $Pt/BaAl_2O_4$-$BaO/\gamma$-$Al_2O_3$ interaction with $CO_2$ during heating to 1300°C (H) and cooling down (C) in 20 vol.% $CO_2$/He; b) $Pt/BaCeO_3$-$BaO/CeO_2$ interaction with $CO_2$ during heating (H) to 1300°C and cooling (C) in 20, 15, 12.5 and 10 vol.% $CO_2$/He (heating rate 10°C/min; cooling rate 5°C/min).

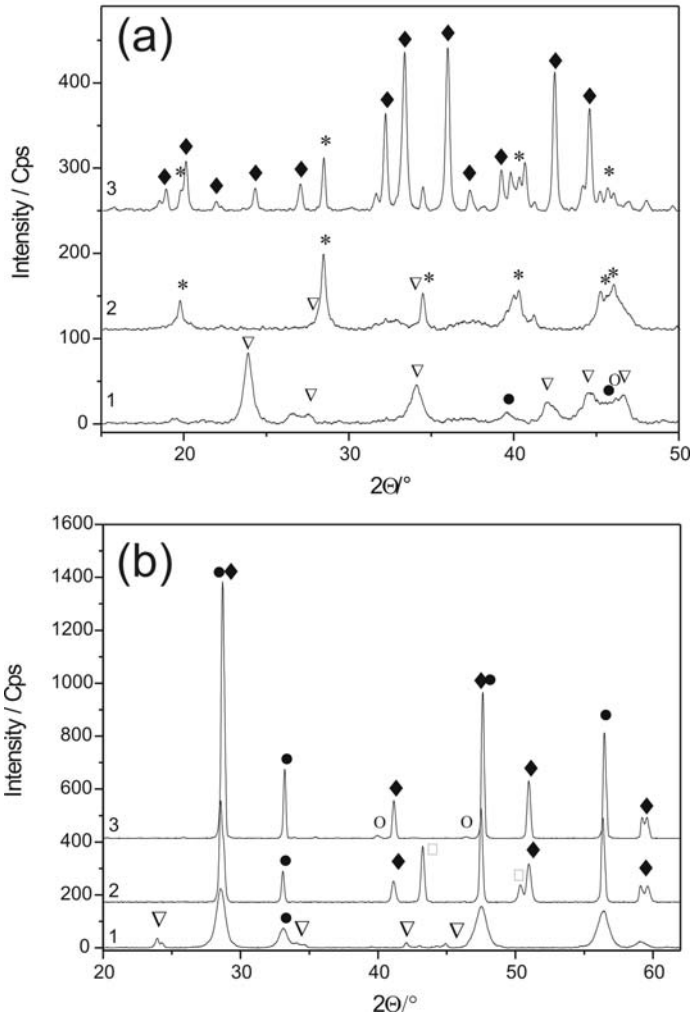


Figure 1

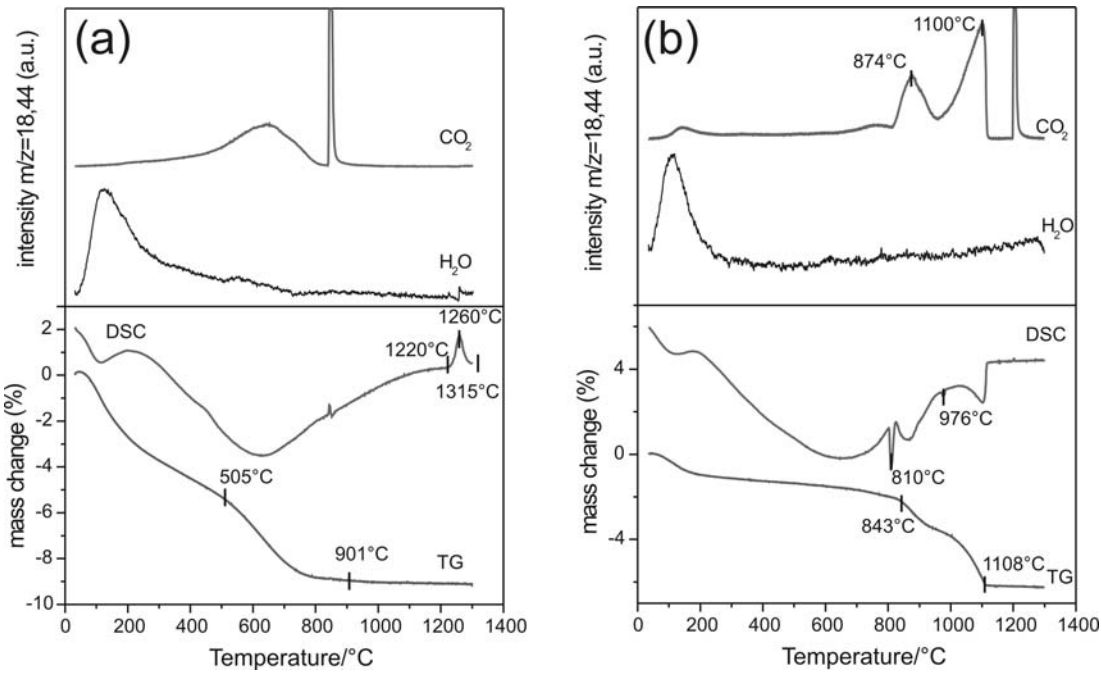
(a)
intensity m/z=18,44 (a.u.)
CO2
H2O
DSC
1260°C
1220°C
1315°C
505°C
901°C
TG
mass change (%)
Temperature/°C
(b)
1100°C
874°C
CO2
H2O
DSC
976°C
810°C
843°C
1108°C
TG
mass change (%)
Temperature/°C

Figure 2

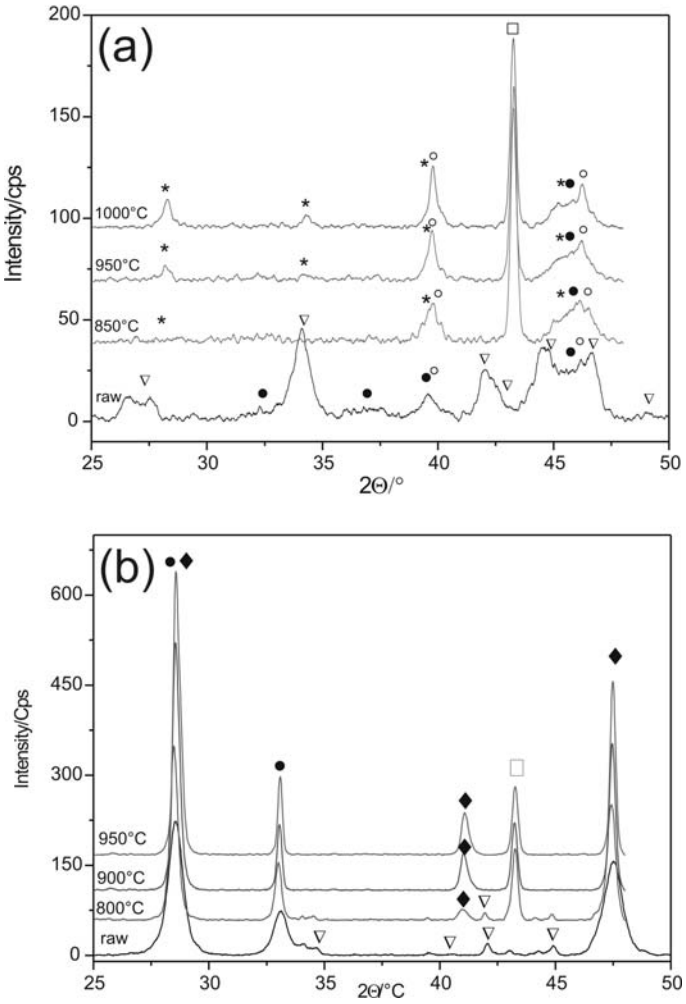
(a)
Intensity/cps
1000°C
950°C
850°C
raw
2Θ/°
(b)
Intensity/Cps
950°C
900°C
800°C
raw
2Θ/°C

Figure 3

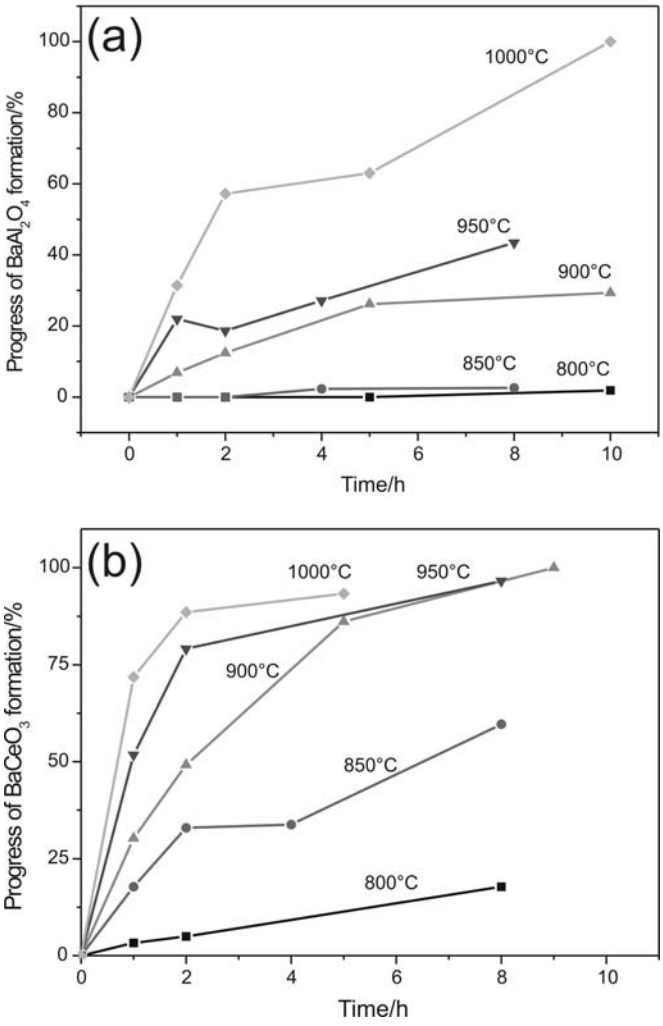
(a)
1000°C
950°C
900°C
850°C
800°C
Progress of $BaAl_2O_4$ formation/%
Time/h
(b)
1000°C
950°C
900°C
850°C
800°C
Progress of $BaCeO_3$ formation/%
Time/h

Figure 4

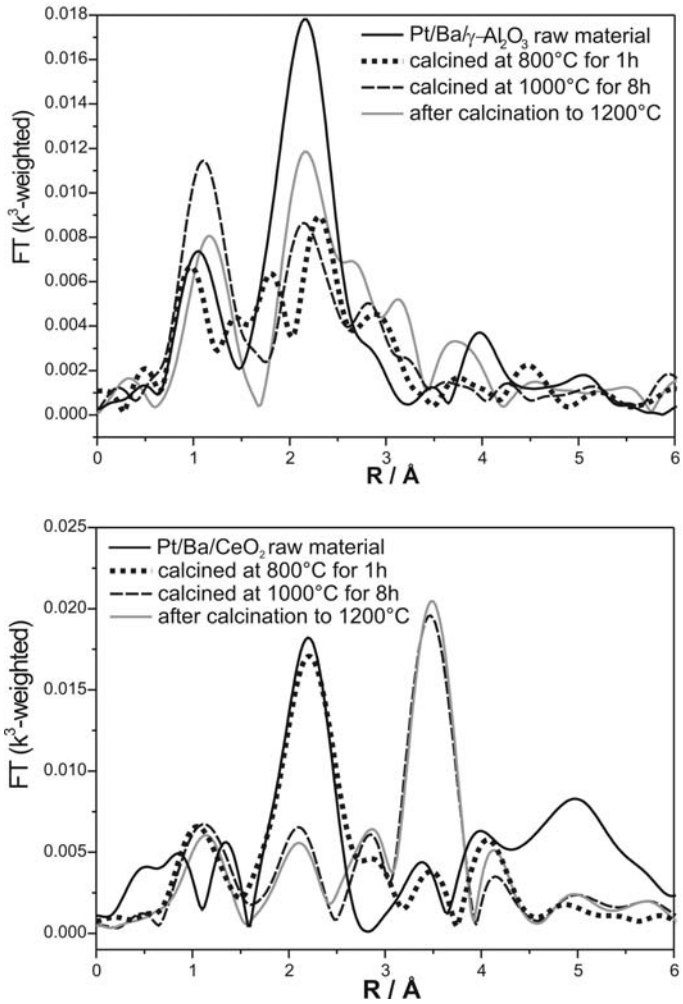
Pt/Ba/γ–Al2O3 raw material
calcined at 800°C for 1h
calcined at 1000°C for 8h
after calcination to 1200°C
FT (k3-weighted)
R / Å
Pt/Ba/CeO2 raw material
calcined at 800°C for 1h
calcined at 1000°C for 8h
after calcination to 1200°C
FT (k3-weighted)
R / Å

Figure 5

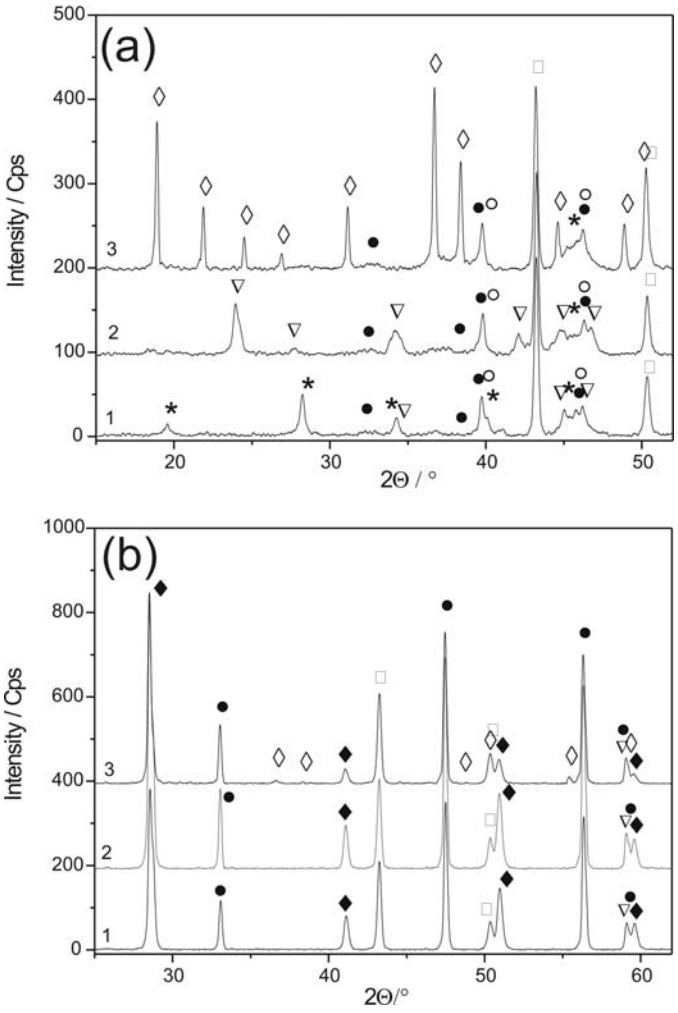


Figure 6

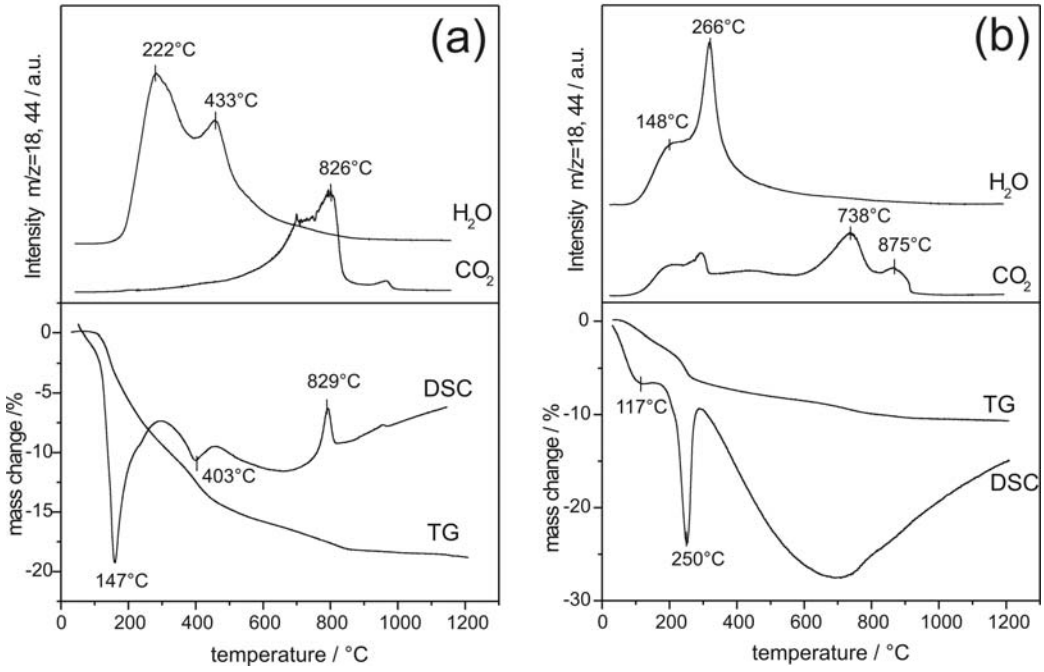
(a)
222°C
433°C
826°C
H2O
CO2
Intensity m/z=18, 44 / a.u.
0
-5
-10
-15
-20
mass change /%
829°C
DSC
403°C
TG
147°C
0
200
400
600
800
1000
1200
temperature / °C
(b)
266°C
148°C
H2O
738°C
875°C
CO2
Intensity m/z=18, 44 / a.u.
0
-10
-20
-30
mass change / %
117°C
TG
DSC
250°C
0
200
400
600
800
1000
1200
temperature / °C

Figure 7

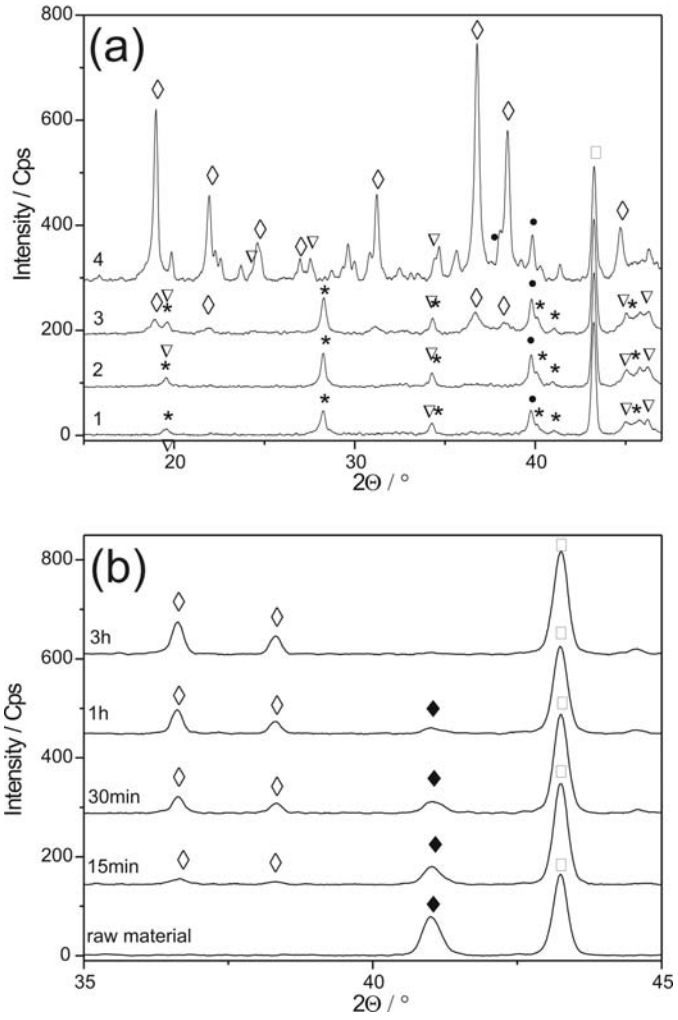


Figure 8

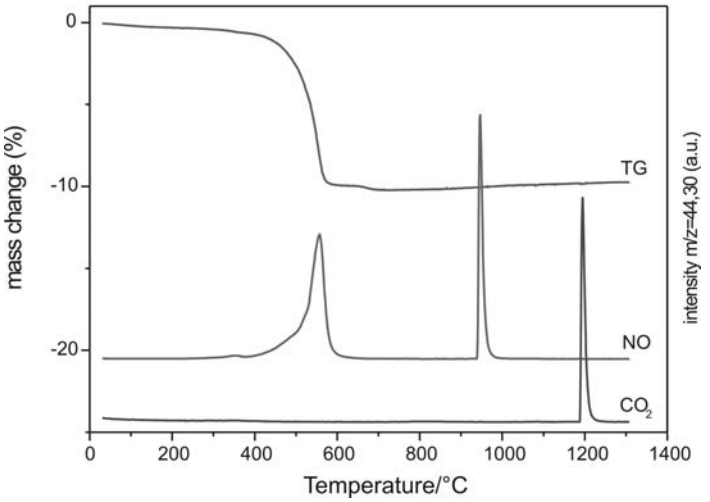
0
-10
-20
mass change (%)
TG
NO
$CO_2$
intensity m/z=44,30 (a.u.)
0
200
400
600
800
1000
1200
1400
Temperature/°C

Figure 9

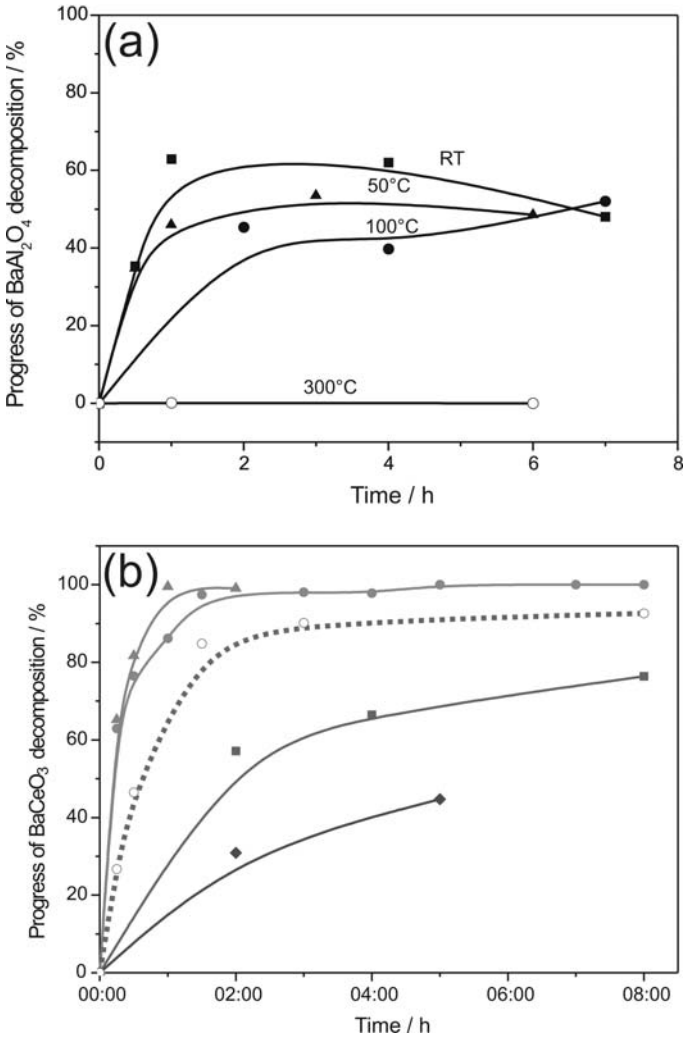
(a)
Progress of $BaAl_2O_4$ decomposition / %
Time / h
RT
50°C
100°C
300°C
(b)
Progress of $BaCeO_3$ decomposition / %
Time / h
00:00
02:00
04:00
06:00
08:00

Figure 10

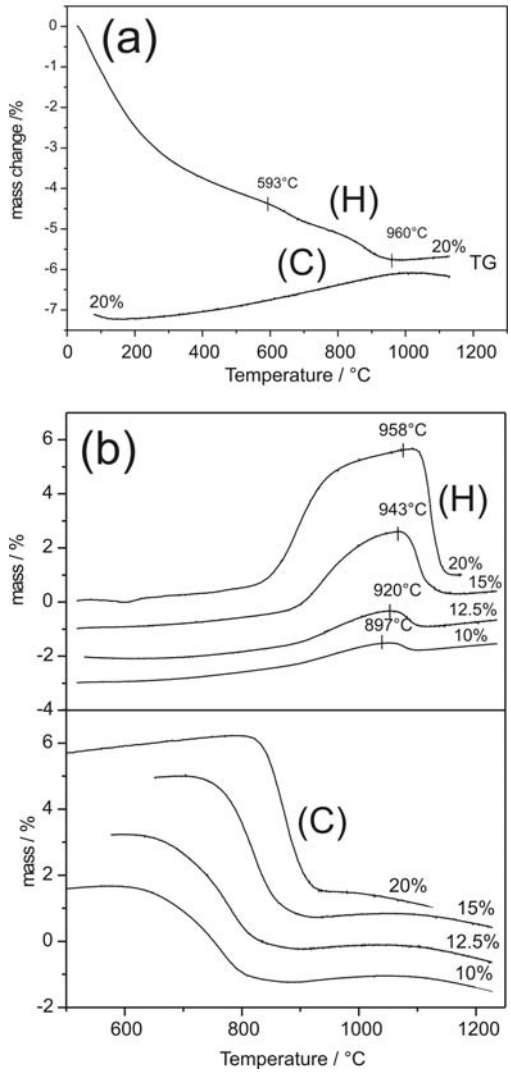
(a)
mass change /%
593°C
(H)
960°C
20%
TG
(C)
20%
Temperature / °C
(b)
958°C
(H)
943°C
20%
15%
920°C
12.5%
897°C
10%
mass / %
(C)
20%
15%
12.5%
10%
Temperature / °C

Figure 11